King's Research Portal

Document Version
Peer reviewed version

[Link to publication record in King's Research Portal](#)

Tools for the efficient implementation of the DBIM algorithm in microwave imaging experiments

Pan Lu*, Juan Córcoles†, Panagiotis Kosmas*

*Department of Engineering, King's College London, London, UK, panagiotis.kosmas@kcl.ac.uk

†Department of Electronic and Communications Technology, Universidad Autónoma de Madrid, Madrid, Spain

Abstract—We present two efficient tools to improve both the experimental data and the reconstruction results in microwave imaging. The time-gating technique can remove part of the unexpected reflections of the cables and tanks, thus improving the quality of the received signals obtained from the experiment system. We also apply the fast iterative shrinkage thresholding algorithm (FISTA) to the distorted Born iterative method (DBIM) as a linear inverse solver at each iteration of the DBIM, which shows better capabilities than the conventional conjugate gradient least squares (CGLS) method with experimental data. Results confirm that the two tools used in the DBIM can be efficient and accurate when employed in the microwave imaging system.

Index Terms—microwave imaging, distorted Born iterative method, time gating, fast iterative shrinkage thresholding, finite difference time domain.

I. Introduction

Microwave imaging (MWI) for medical applications is gaining increasing interest from various research groups worldwide, as it is safe, non-invasive, and has potential to lead to low-cost and portable devices [1]. MWI methods reconstruct the distribution of tissues with different electric properties by solving an electromagnetic inverse scattering problem [2].

As the MWI imaging system consists mainly of two components, the data acquisition system and the imaging method [3], [4], it is important to both improve the accuracy of the data obtained from the data acquisition system and use an efficient algorithm to solve the ill-posed linear system. The experimental data is usually obtained from a vector network analyzer (VNA) and can be improved by signal processing techniques such as time gating [5], resulting in a further improvement of the reconstruction results. With regards to the inverse problem, our recent work [6] has shown that the fast iterative shrinkage thresholding algorithm (FISTA) used as linear solver in the distorted Born iterative method (DBIM) can improve the reconstruction results with simulation data compared with the traditional inverse solver CGLS. Moreover, compared with the two-step iterative shrinkage thresholding (TwIST) algorithm, FISTA is easier to control as it has fewer parameters than TwIST. In this work, we employ the DBIM-FISTA algorithm to experimental data processed by the time gating technique in simplified two-dimensional (2D) cross-section geometries of the three-dimensional (3D) problem.

The remainder of this work is organized as follows: In Section II, we review the formulation of the DBIM and FISTA in MWI. The time gating technique to process the data obtained from our experimental system is introduced in Section III with an example showing the comparison between the original and processed data in time and frequency domain. Reconstructions with the experimental data are presented in Section IV, followed by conclusions in Section V.

II. Methods

A. Distorted Born Iterative Method (DBIM)

The DBIM is an iterative inverse scattering algorithm which is commonly used to estimate the spatial distribution of dielectric properties within a region V [2]. It is based on a non-linear integral equation which can be approximated via the Born approximation as,

$$E_s(\boldsymbol{r_n}, \boldsymbol{r_m}) = E(\boldsymbol{r_n}, \boldsymbol{r_m}) - E_b(\boldsymbol{r_n}, \boldsymbol{r_m})$$
$$= \omega^2 \mu_0 \varepsilon_0 \int_V G_b(\boldsymbol{r_n}, \boldsymbol{r}) E_b(\boldsymbol{r}, \boldsymbol{r_m}) \delta_\varepsilon(\boldsymbol{r}) d\boldsymbol{r}, \quad (1)$$

where E_s, E_b are the scattered and background fields respectively, $\boldsymbol{r_n}$ and $\boldsymbol{r_m}$ are the transmitting and receiving antenna locations, ω is the angular frequency, μ_0 is the relative permeability, ε_0 is the relative permittivity, and G_b is the Green's function for the background medium. The contrast δ_ε between the relative complex permittivities of the reconstruction domain $\varepsilon(\boldsymbol{r})$ and background $\varepsilon_b(\boldsymbol{r})$ is defined as $\delta_\varepsilon(\boldsymbol{r}) = \varepsilon_r(\boldsymbol{r}) - \varepsilon_b(\boldsymbol{r})$.

The integral equation (1) can be discretized for all transmit-receive pairs, leading to an under-determined and ill-posed linear system,

$$A\delta_\varepsilon(\boldsymbol{r}) = b \quad (2)$$

where A is an $M \times N$ matrix, with M transmit-receive pairs and N voxels in the reconstruction region V, b is a $M \times 1$ vector of the scattered fields. At each DBIM iteration i after calculating the background field by the forward solver, the linear problem (2) is solved by the inverse solver and the background permittivity is updated by $\varepsilon_b^{i+1}(\boldsymbol{r}) = \varepsilon_b^i(\boldsymbol{r}) + \delta_\varepsilon(\boldsymbol{r})$.

As A is severely ill-posed and under-determined, i.e. $M \ll N$, (2) cannot be solved easily by direct methods. Instead, iterative solvers are used to obtain a reliable solution such as the CGLS algorithm [7] or the TwIST/FISTA [6], [8].
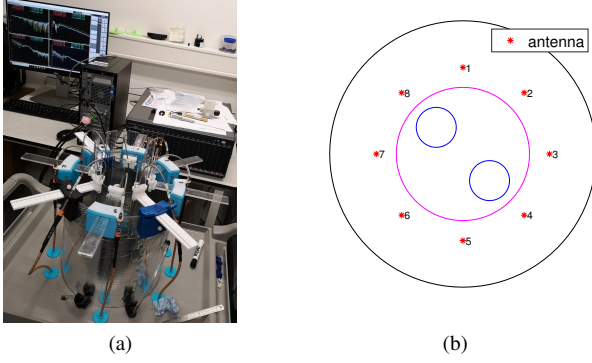
Fig. 1. (a) The experimental system. (b) The configuration (top view): inner tank (radius 5 cm, marked in a magenta circle), outer tank (radius 10 cm, marked in a black circle), two targets (radius 1.5 cm, marked in blue circles) and antennas (placed in a circle with radius 6.5 cm, marked in red).

B. Fast Iterative Shrinkage Thresholding Algorithm (FISTA)

To solve the ill-conditioned linear system $Ax = b$ directly, a minimization problem $\min_x \|Ax - b\|^2$ is usually considered. The FISTA can be used to solve this minimization problem at each DBIM iteration, which obtains the solution by minimizing the following object function based on the l_p–norm $\| \cdot \|_p = \sqrt[p]{| \cdot |^p}$,

$$F(x) = \frac{1}{2}\|Ax - b\|_2^2 + \lambda\|x\|_p \qquad (3)$$

where λ is a regularization parameter, and usually the l_1-norm or l_2-norm is chosen. In this work, the l_1–norm is used. This minimization problem (3) in MWI can be solved by various methods including different types of iterative thresholding methods [8], [9]. The FISTA is based on [10], which uses the accelerated Nesterov's momentum to improve efficiency and convergence rate. The structure of the FISTA is constructed as,

$$\begin{aligned} x_k &= p_L(y_k), \\ t_{k+1} &= \frac{1 + \sqrt{1 + 4t_k^2}}{2}, \\ y_{k+1} &= x_k + \frac{t_k - 1}{t_{k+1}}(x_k - x_{k-1}) \end{aligned} \qquad (4)$$

where $t_0 = 1$, p_L is the soft thresholding function, and y_k is the solution at the k–th iteration.

III. EXPERIMENTAL DATA PREPROCESSING

The experimental data was obtained from our previous proposed experimental system [4], which uses an eight-port VNA to record simultaneously the signals received from an 8-antenna circular ring when one of them transmits. In the experiment, the tank is filled with a homogeneous background medium, which is a glycerol(90%)-water(10%) mixture. The permittivity of the glycerol-water mixture is $\varepsilon_r \approx 16 - 15j$ at 1 GHz. The radii of the antenna array and the reconstruction domain are $\rho_{ant} = 6.5$ cm and $\rho_R = 5.0$ cm respectively. The frequency range in this work used for reconstruction is between 0.5 GHz and 1.0 GHz. The general configuration of

the experiment system from the top view is shown in Fig. 1, where antennas are numbered in clockwise order. To remove the unexpected reflections by the cables and tanks in the experimental system, the time gating technique is employed, to test if it can improve the quality of the S-parameters obtained by the VNA by producing time-gated data that resembles more the signals reflected by the target.

To process the frequency-domain data, the data is first converted to the time domain by using the inverse Fourier transform (IFT). The point with the peak value is set to be the center point of the gate function and a time span is chosen. Thus the window function for time gating is built in the time domain and converted back to the frequency domain by the Fourier transform. The frequency-domain window function is convolved with the original data to obtain the time-gated data.

In Figs. 2 and 3, an example where there is only the homogeneous background medium is shown by using the above time-gating technique to process the S-parameter S_{41}, where the time span is set to be 30 ns. The time domain data is plotted with the use of a Hamming window function. As can be seen from Fig. 2, most of the reflections after the peak value are removed by the window function. As for the frequency-domain data, the plotting curve of the gated data is much more stable than the original data. For the reconstructions with processed data in the next section, the same criteria for processing the original data are used to obtain the gated data.
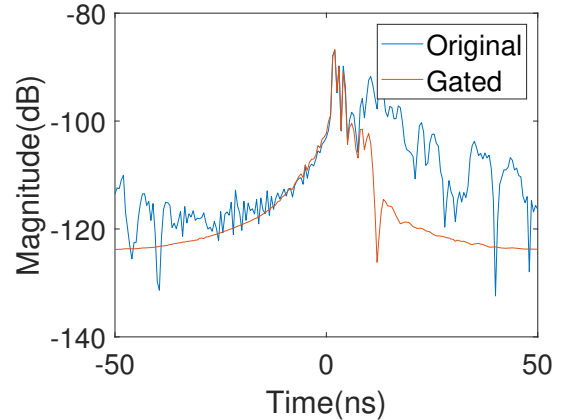

Fig. 2. Magnitude in dB of the S-parameter S_{41} in time domain.

IV. RECONSTRUCTION RESULTS

In this section, reconstruction results with experimental data are shown and the results of original and processed data are compared. The comparison between the reconstruction results with CGLS and FISTA are also presented. All the reconstructions are performed by using the finite difference time domain (FDTD) method with the convolutional perfectly matched layer (CPML) as a forward solver for the DBIM. The single-pole Debye model is employed as,

$$\varepsilon_r(\omega) = \varepsilon_\infty + \frac{\Delta\varepsilon}{1 + j\omega\tau} + \frac{\sigma_s}{j\omega\varepsilon_0}. \qquad (5)$$
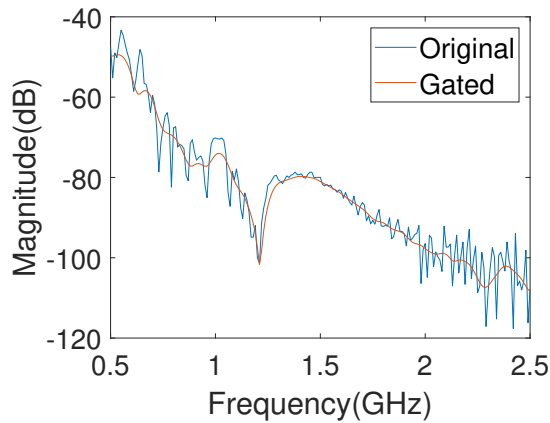
Fig. 3. Magnitude in dB of the S-parameter S_{41} in frequency domain.

reconstruction results. With the time gating, the S-parameters obtained the experimental system can be more smooth and accurate. By using the FISTA algorithm as an inverse solver for the DBIM, the targets can be reconstructed with better resolution and less noise.

where ε_∞, $\Delta\varepsilon$, τ and σ_s are the parameters of the Debye model. After reconstruction, the Debye parameters are used to calculate the complex permittivity. The total domain size for the FDTD method is 100×100 voxels, with each voxel size 2 mm $\times$ 2 mm.

The experiments include two scenarios: one is a single cylindrical target placed at (-2 cm, 2 cm) inside a tube filled with pure water, while the other one consists of two targets placed at (∓ 2 cm, $\pm$ 2cm) in the same configuration. The permittivity of pure water is $\varepsilon_{target} \approx 78 - 3j$, and the radius of each target is $\rho_{target} = 1.5$ cm.

The real part of the permittivity of the reconstruction results is shown in Fig. 4 and Fig. 5, where the reconstruction domain and the exact target size are marked in a magenta circle and a black circle respectively. For each one, 20 DBIM iterations are performed with the CGLS algorithm or the FISTA. To evaluate the CGLS algorithm and FISTA fairly, the same number of iterations inside the inverse solver are used, which is set to be 75. The figures in the first row, the second row and the third row are the reconstruction results with original data by FISTA, with processed data by CGLS, and with processed data by FISTA respectively. Comparing the first row with the third row, the results with processed data have been improved significantly, especially at 0.6 GHz and 0.7 GHz, where the the targets are not detected with the original data. Compared with the reconstruction results by CGLS, the results in the third row by FISTA have less noise and the resolution has also been improved.

V. CONCLUSION

We have presented two efficient tools that can be used for the inverse scattering problem in MWI to improve the

REFERENCES

[1] P. Kosmas and L. Crocco, "Introduction to special issue on Electromagnetic technologies for medical diagnostics: Fundamental issues, clinical applications and perspectives," *Diagnostics*, vol. 9, no. 1, p. 19, 2019.

[2] D. W. Winters, J. D. Shea, P. Kosmas, B. D. Van Veen, and S. C. Hagness, "Three-dimensional microwave breast imaging: Dispersive dielectric properties estimation using patient-specific basis functions," *IEEE Transactions on Medical Imaging*, vol. 28, no. 7, pp. 969–981, July 2009.

[3] S. Semenov, "Microwave tomography: review of the progress towards clinical applications," *Philosophical Transactions of the Royal Society A: Mathematical, Physical and Engineering Sciences*, vol. 367, no. 1900, pp. 3021–3042, 2009.

[4] S. Ahsan, Z. Guo, Z. Miao, I. Sotiriou, M. Koutsoupidou, E. Kallos, G. Palikaras, and P. Kosmas, "Design and experimental validation of a multiple-frequency microwave tomography system employing the DBIM-TwIST algorithm," *Sensors*, vol. 18, no. 10, p. 3491, 2018.

[5] B. Archambeault, S. Connor, and J. C. Diepenbrock, "Time domain gating of frequency domain S-parameter data to remove connector end effects for PCB and cable applications," in *2006 IEEE International Symposium on Electromagnetic Compatibility, 2006. EMC 2006.*, vol. 1, Aug 2006, pp. 199–202.

[6] P. Lu, J. Córcoles, and P. Kosmas, "Non-linear microwave imaging using fast iterative shrinkage thresholding," in *2019 Progress in Electromagnetics Research Symposium (PIERS-Rome)*, June 2019.

[7] T. Rubæk, P. M. Meaney, P. Meincke, and K. D. Paulsen, "Nonlinear microwave imaging for breast-cancer screening using Gauss-Newton's method and the CGLS inversion algorithm," *IEEE Transactions on Antennas and Propagation*, vol. 55, no. 8, pp. 2320–2331, Aug 2007.

[8] Z. Miao and P. Kosmas, "Multiple-frequency DBIM-TwIST algorithm for microwave breast imaging," *IEEE Transactions on Antennas and Propagation*, vol. 65, no. 5, pp. 2507–2516, 03 2017.

[9] M. Ambrosanio, P. Kosmas, and V. Pascazio, "A multithreshold iterative DBIM-based algorithm for the imaging of heterogeneous breast tissues," *IEEE Transactions on Biomedical Engineering*, vol. 66, no. 2, pp. 509–520, Feb 2019.

[10] A. Beck and M. Teboulle, "A fast iterative shrinkage-thresholding algorithm for linear inverse problems," *SIAM Journal on Imaging Sciences*, vol. 2, no. 1, pp. 183–202, 2009. [Online]. Available: https://doi.org/10.1137/080716542
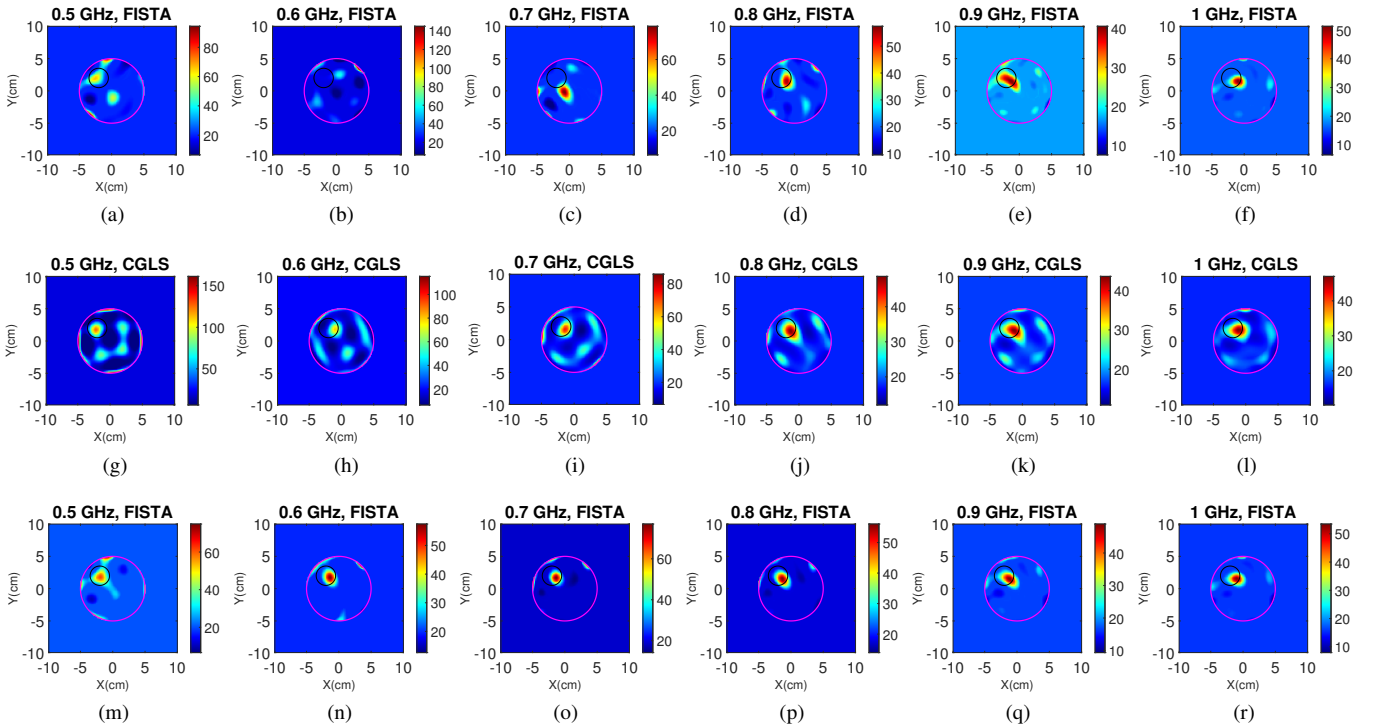
Fig. 4. Reconstruction results of real permittivity of one target by 20 DBIM iterations. The first row (a) – (f): reconstructed by FISTA with original data. The second row (g) – (l): reconstructed by CGLS with processed data. The third row (m) – (r): reconstructed by FISTA with processed data.
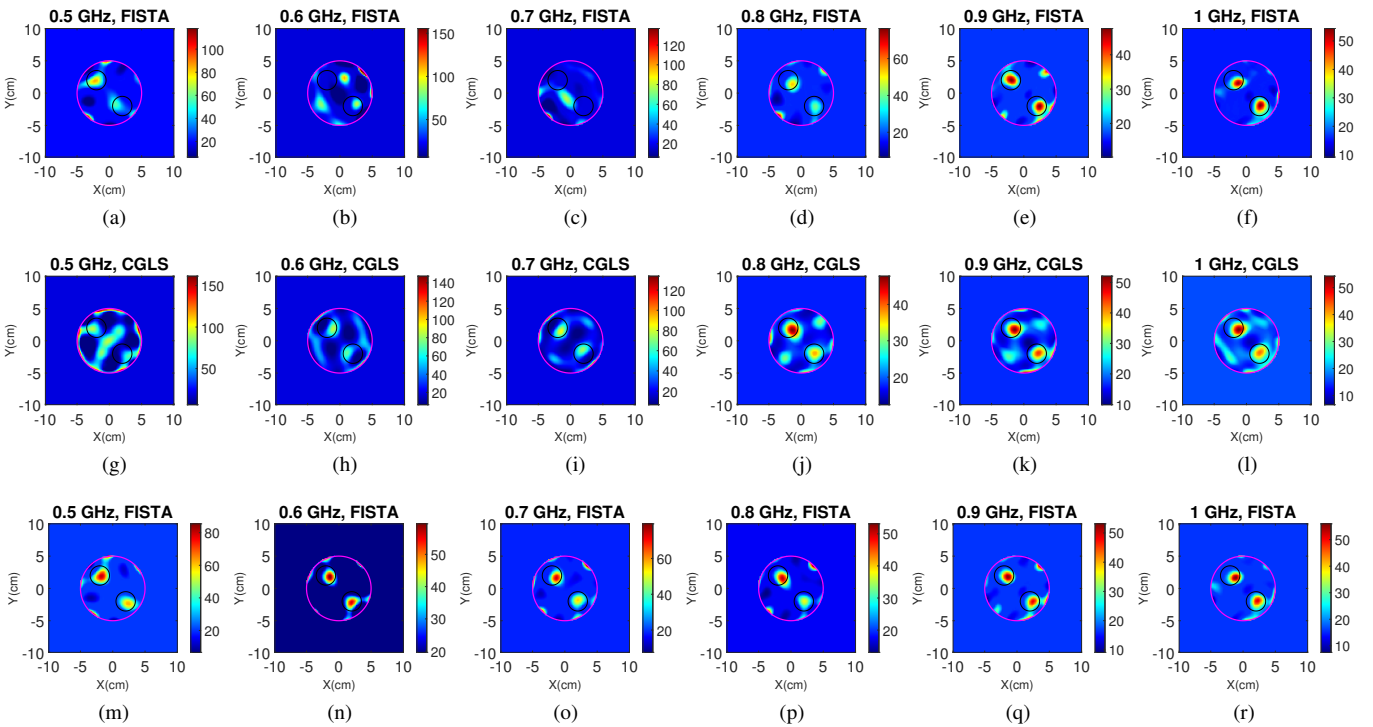

Fig. 5. Reconstruction results of real permittivity of two targets by 20 DBIM iterations. The first row (a) – (f): reconstructed by FISTA with original data. The second row (g) – (l): reconstructed by CGLS with processed data. The third row (m) – (r): reconstructed by FISTA with processed data.